

Determination of fibre–matrix interfacial properties in ceramic–matrix composites by a fibre push-out technique

R. N. SINGH, M. SUTCU

General Electric Corporate Research and Development, P.O. Box 8, Building K-1, Room 4A32, Schenectady, NY 12301, USA

A simple concentric cylinder model is developed for the fibre push-out test in order to interpret the experimentally observed indenter load–displacement curves in ceramic–matrix composites. The fibre–matrix interface is assumed to be partially bonded and partially frictionally coupled. It is shown that a slope change in the loading curve corresponds to bonding at the fibre–matrix interface. In contrast, an insignificant change in the slope is predicted for composites in which the fibre–matrix interface is frictionally coupled. This model also provides a framework for determining the interfacial debond energy and the interfacial shear strength in ceramic composites using the fibre push-out tests. The predictions of this model are compared with the push-out test results performed on zircon–SiC composites uniaxially reinforced with either uncoated or BN-coated SiC monofilaments, which suggested that the fibre–matrix interfaces in both of these composites are frictionally coupled.

1. Introduction

The mechanical properties of a continuous fibre–reinforced ceramic–matrix composite (CMC) are dependent on properties of the reinforcement and the matrix materials, processing conditions, and the fibre–matrix interfacial properties. In particular, the first matrix cracking stress and the toughness are dependent on the fibre–matrix interfacial shear stress. Generally, a weakly bonded fibre–matrix interface results in a toughened composite-like behaviour because of the fibre pull-out mechanism, whereas a strongly bonded fibre–matrix interface creates a brittle composite. Theoretical analysis [1, 2] and experimental results [3–6] have shown that an optimal value of the interfacial shear strength can lead to ceramic composites with a significant enhancement in strength and toughness over that attainable for monolithic ceramics. Therefore, a knowledge of the fibre–matrix interfacial shear strength in CMCs is essential for designing toughened composites.

The fibre–matrix interfacial shear strength has been measured in CMCs by a number of techniques, such as microindentation [7], fibre push-out [8–10], fibre pull-out [11], and single-fibre tensile testing [12]. Among these techniques, the fibre push-out method is most easily performed and gives the most direct measurement of the debond and frictional components of interfacial shear stress. The fibre push-out method has been used to demonstrate the effects of fibre–matrix interaction [9], thermal expansion mismatch between the fibre and the matrix [8], and composite processing conditions [4] on the measured values of interfacial shear stress. In addition, reinforcement coatings have been used to modify interfacial

properties that in turn have been shown to influence mechanical properties [4, 6].

A detailed analytical model of the fibre push-out technique, similar to that developed for the micro-indentation technique [7], is not available in the literature. Therefore, one of the objectives of this study was to develop a micromechanical model for the fibre push-out test. The predictions of this model were compared with the push-out test results performed on zircon–SiC composites uniaxially reinforced with either uncoated or BN-coated Avco SCS-6 silicon carbide monofilaments. Analysis of the push-out test results, with respect to the analytical model, has provided additional insight into the nature of fibre–matrix interfacial bond. Specifically, an attempt was made to determine experimental observations that can be used as evidence of fibre–matrix interfacial bonding.

2. Experimental procedure

The fibre push-out experiments were performed on a zircon ($ZrSiO_4$) matrix composite uniaxially reinforced with Avco SCS-6 silicon carbide monofilaments. These filaments were fabricated by a chemical vapour deposition technique in which SiC was deposited on a carbon fibre core of about 37 μm diameter, followed by depositions of two layers of carbon-rich coatings of 3 μm thickness. This results in an overall fibre diameter of 140 μm . Typical mechanical properties of these filaments at room temperature are: a strength of 3.4 GPa, modulus of 400 GPa, and failure strains between 0.8 and 1.0%. Two types of

fibre-matrix interface were created in fully consolidated composites. In one case, as-supplied SiC monofilaments were used in the zircon matrix, thereby creating an interface (interface A) between the outer carbon layer and the zircon matrix. In another case, BN-coated SiC monofilaments were incorporated into the zircon matrix, thus creating another interface (interface B) between the BN coating and the zircon matrix. The BN coating of about 1 μm thickness was deposited on SiC filaments by a low-pressure chemical vapour deposition technique (LPCVD) [13]. The coefficient of thermal expansion of both the fibre and the matrix is $4.2 \times 10^{-6}(\text{°C})^{-1}$. Thus, the thermal stresses are eliminated.

Composite samples reinforced with either as-supplied or BN-coated filaments were fabricated by aligning filaments uniaxially and then incorporating zircon matrix around each of the filaments. The final consolidation was done by hot-pressing between 1500 and 1600 °C , which resulted in fully dense composites with little ($< 1\%$) porosity. Typically, composites with 25 vol % filaments were produced for the fibre push-out experiments of this study.

The fibre push-out technique was used to measure fibre-matrix interfacial shear strength. In this technique, a thin slice (1 to 2 mm thick) was cut perpendicular to the filament axis and polished in such a way as to produce a small amount of filament relief on one side (typically 0.06 to 0.1 times the fibre diameter). This was achieved in the case of zircon-SiC composites by polishing both surfaces, initially using diamond pastes on a hard polishing wheel, followed by the final polishing of one of the surfaces with a soft cloth using fine alumina polishing powder to produce filament relief. This thin slice was then placed on a rigid substrate having a small opening, and the filament to be pushed was aligned over this opening. Subsequently, the filaments were individually loaded by an indenter (as shown in Fig. 1) at a constant displacement rate until the first evidence of filament motion was observed. The first evidence of filament motion was detected by a sudden load drop in the load-deflection curve, which was generated by measuring the load by a load-cell when pushing on the filament at a constant displacement rate. Experiments were performed at different displacement rates to study the influence of stressing rate on interfacial shear-stress measurements. After the first push, the sample was turned over, and measurements were repeated on already pushed filaments. The load to move the filaments for the second time was invariably lower than that for the first push. Typically, 10 to 15 filaments were pushed in each sample to obtain an average value of the interfacial shear stress. Composites reinforced with as-supplied and BN-coated SiC monofilaments were used in the fibre push-out experiments to study the influence of BN coating in modifying the fibre-matrix interfacial properties and associated changes in the load-deflection data (as determined during the push-out tests).

The fibre-matrix interface can be bonded by either a chemical bond or by a frictional force. Generally, chemical bonds are produced because of reaction

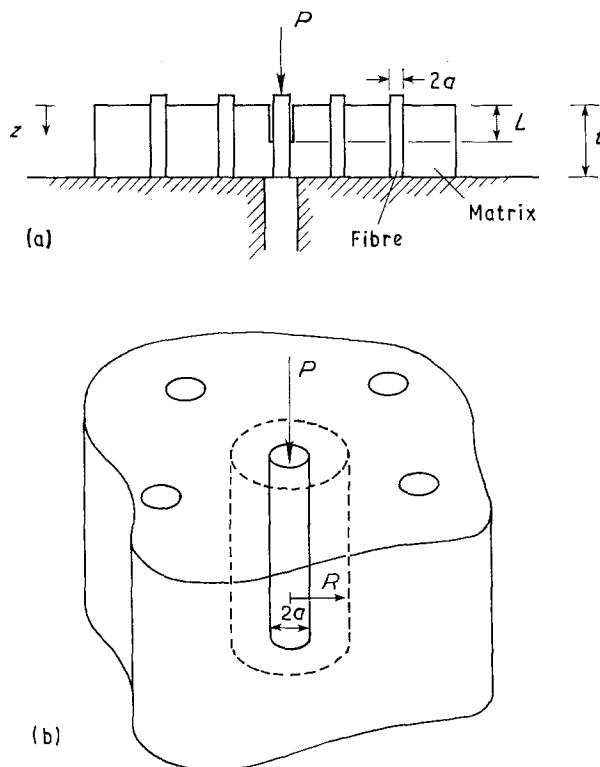


Figure 1 Schematic diagrams showing (a) the experimental arrangement for fibre push-out tests, and (b) the composite material around the fibre, which is approximated by a concentric cylinder with radius R .

and/or interdiffusion between the constituents comprising the fibre and the matrix phase, and can lead to a significant amount of fibre-matrix adhesion. In contrast, a frictionally coupled fibre-matrix interface will be weakly bonded because of the nature of the Coulomb friction. The frictional force τ is a product of the friction coefficient (μ) and the normal force (σ_r) in the radial direction. The normal stress can arise as a result of the thermal expansion mismatch between the fibre and the matrix and/or because of the mechanical interlocking between the interfaces. When the fibres are pushed for the second time, only the frictional component should be operable because the bonds have already been broken on the first push. For the second push, then

$$\tau_2 = \mu \sigma_r.$$

The friction coefficient μ during the second push may be different from the first push value. Some of the composite samples were pushed for the third time to determine the changes in interfacial properties caused by the accumulation of frictional damage at the sliding fibre-matrix interfaces.

3. Analytical model

In this section we will present a simple concentric cylinder model in order to predict analytically the indenter load-displacement curves. The input into the model consists of the fibre and the matrix material properties, the volume fractions, the thickness of the test sample, and the experimentally determined load values during the push-out test. In return, we would like to compute the indenter load-displacement

curves, the interface debond energy (if any), and the frictional shear stress. The fibre-matrix interface is assumed to be partially debonded and partially bonded. The debonded portion is assumed to be weakly coupled by friction, whereas the bonded portion is relatively strongly bonded because of the chemically induced adhesive force.

We expect to see three separate regions in a typical load-displacement curve in a fibre push-out experiment. In the first region, the applied load causes elastic depression of the fibre and the surrounding matrix without the interface motion. This will be the case regardless of the nature of the interface bonding. The second region occurs after the applied load reaches a sufficiently high value to initiate either debonding or frictional sliding. In the third region, the fibre is frictionally sliding along its entire length and the load decreases. It should be mentioned that in the case of a frictionally coupled interface the first region associated with elastic depression may be very small.

A schematic diagram of the fibre push-out test is given in Fig. 1a, in which a composite slice of thickness t is placed on an elastic base, while a force P is applied to the end of the fibre. This situation is close to the problem of a concentrated force on an elastic half-space [14], in which the stresses in the vicinity of the applied force drop very rapidly in the radial as well as in the axial directions. In particular, the shear stress drops with the third power of the axial distance z and with the fourth power of the radial distance r .

A rigorous analysis of the situation in Fig. 1a is complex. However, our purpose is to compute the energy changes associated with axial stresses alone. We do not make an effort to compute the radial and the hoop-stress distributions. Therefore, it may be sufficient to consider a finite concentric cylinder model to approximate the local deformation behaviour at the point of application of the force P . To achieve this, it is assumed that a small cylindrical region around the fibre carries most of the load, as shown in Fig. 1b. Therefore, we propose to replace the infinite composite around the fibre that is being pushed by a composite jacket with a finite outer radius R given by

$$R = a3^{1/2} \quad (1)$$

where a denotes the fibre radius. The elastic properties of this jacket are the same as those of the composite. The chosen radius R in Equation 1 reproduces the exact ratio of the axial stress and the shear stress for an elastic half-space under a concentrated load [14] in the matrix near the interface. Physically, this assumption is equivalent to replacing the elastic support under the composite test slice with a hollow cylinder with an inner radius a and an outer radius R . It can be shown that the analysis is not very sensitive to the rather arbitrary choice of R in Equation 1. Qualitatively, this is because of the very rapid decay of stresses with the radial distance r from the fibre. A uniaxially reinforced composite has five independent elastic constants. The axial shear modulus of the composite can be calculated [16], and is approximately equal to the shear modulus of the matrix, G . The model is further simplified by concentrating all the axial stress-carry-

ing area of the matrix at an effective radius \bar{R} between a and R , and assuming that the region in $a \leq r \leq R$ supports only shear stress $\tau(r, z)$, as was done by Budiansky *et al.* [1]. The radius \bar{R} is calculated from energy arguments based on a certain shear stress distribution [1] and is approximately given by

$$\log(\bar{R}/a) = v/2 = 1/4 \quad (2)$$

where the quantity v is introduced for mathematical convenience in order to use some of the results from earlier work [15].

The stresses for the concentric cylinder model shown in Fig. 2 decay exponentially with distance z in the bonded elastic region, as predicted by Budiansky *et al.* [1]. The coefficient that multiplies distance z in the exponent was denoted by ρ [1]. The expression for ρ for the composite cylinder model in Fig. 2 is given by

$$\rho^2 = \frac{2G}{v} \left(\frac{1}{E} + \frac{2}{E_f} \right) = 4G \left(\frac{1}{E} + \frac{2}{E_f} \right) \quad (3)$$

where E and E_f are Young's moduli of the composite and the fibre, respectively. The axial composite modulus is approximated by the rule of mixtures:

$$E = V_f E_f + V_m E_m \quad (4)$$

where E_m denotes the matrix Young's modulus. The fibre and the matrix volume fractions V_f and V_m are not related to the choice of radius R in Equation 1. The stress decay parameter ρ in Equation 3 is used in the next section where we give the stresses.

3.1. Stresses in the debonded region

It is assumed that the force P is positive when it is pushing on to the fibre, as shown in Fig. 2. Debonding

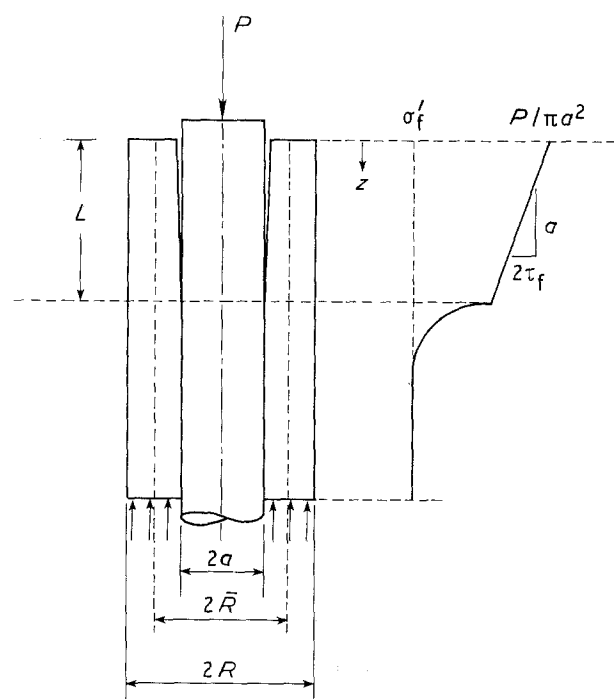


Figure 2 Axial fibre stress profile in the composite cylinder. A linear profile is shown along the debonded length L where frictional sliding occurs. In the bonded region the stress decays exponentially to the level of the thermal stress σ_f' . We neglect elastic stress recovery at the bottom end.

is assumed to have taken place over a distance L . The axial fibre stress σ at the point of application of the force P at $z = 0$ is given by

$$\sigma = \sigma_f(0) = -P/\pi a^2 \quad (5)$$

In the debonded region ($0 \leq z \leq L$), the fibre and the matrix axial stresses, $\sigma_f(z)$ and $\sigma_m(z)$, and the interface shear stress, $\tau_i(z)$, are governed by

$$\begin{aligned} \sigma_f(z) &= \sigma + 2\tau_f(z/a) \\ \sigma_m(z) &= -\tau_f z/a \\ \tau_i(z) &= -\tau_f \end{aligned} \quad (6)$$

where $0 \leq z < L$. For the derivation of these stresses, see Budiansky *et al.* [1].

3.2. Stresses in the bonded region

The stresses beyond the slip region, where $z > L$, are given by [15]

$$\begin{aligned} \sigma_f(z) &= \sigma'_f + \frac{2\tau_i}{\rho} \\ \sigma_m(z) &= \frac{\sigma}{2} - \frac{\sigma'_f}{2} - \frac{\tau_i}{\rho} \\ \tau_i(z) &= -\tau_d \exp\left(-\rho \frac{z-L}{a}\right) \end{aligned} \quad (7)$$

The term τ_d is the debond shear strength of the interface. The term σ'_f is the residual fibre stress that may have resulted from composite processing and/or expansion mismatch between the fibre and the matrix. The tensile residual stresses have positive values. In deriving the stresses in Equation 7 we assumed that the test specimen is infinitely long in the fibre direction. It has been shown [15] that the elastic end-effects die out over a distance which is a fraction of the fibre radius. Thus, we ignore the elastic stress recovery at the opposite end of the test specimen in Fig. 1a.

The requirement that the axial stresses be continuous in the matrix and the fibre at the end of the slip region where $z = L$ gives an estimate of the debond length L [15, 1]:

$$\frac{L}{a} = \frac{-\sigma + \sigma'_f}{2\tau_f} - \frac{\tau_d}{\tau_f \rho} \quad (8)$$

in terms of the applied fibre stress σ and the interface shear strength τ_d . Later, we will express the debond length L in Equation 8 in terms of the force P and the interface debond energy Γ_d .

3.3. Debond shear strength and force of debonding P

Our approach is to equate the external work done by the force P to the sum of three energy/work terms, namely, the change in the elastic energy of the system, the frictional dissipation along the debonded length, and the energy Γ_d consumed to separate the interface. This is readily done by the analysis presented elsewhere [15]. The results presented here were obtained by setting the fibre and the matrix volume fractions

equal to 1/3 and 2/3, respectively, and $v = 1/2$ in accordance with the choice of the outer radius R in Equation 1. The interface shear strength τ_d is a constant for a given composite material and related to the interface debond energy Γ_d as follows [15]:

$$\tau_d - \tau_f = (8G\Gamma_d/a)^{1/2} \quad (9)$$

The relationship between the debond length L and the force for debonding P can be obtained from Equation 8 by eliminating τ_d and σ using Equations 9 and 5, respectively:

$$\frac{P}{\pi a^2} = -\sigma'_f + 2\tau_f \left(\frac{L}{a} + \frac{1}{\rho}\right) + \frac{4}{\rho} \left(\frac{2G\Gamma_d}{a}\right)^{1/2} \quad (10)$$

This expression, without the thermal residual stress σ'_f , is essentially the same as the equivalent relationship that can be derived using Marshall's push-in model [7]. The differences are a multiplication constant that multiplies the debond energy Γ_d in the last term and the elastic term $2\tau_f/\rho$, in comparison with Marshall and Oliver [7].

The force required to initiate debonding is obtained from Equation 10 by setting the debond length L equal to zero. If the predicted value from Equation 10 is negative, then this may be an indication that the composite has already debonded because of the axial residual fibre stress σ'_f . The force required for further debonding increases linearly with L with a slope governed by the frictional shear stress τ_f . The model is no longer accurate as the debond length L approaches the specimen thickness t within a few fibre radii. Nevertheless, the maximum force for debonding in this model occurs when the length L is equal to the specimen thickness t in Equation 10.

3.4. Relationship between force of the indenter and fibre displacement

The relationship between the force P and the displacement of the indenter, denoted by u , is governed by the fibre displacement, which is obtained from Equations 6 and 7 by expressing the axial stress $\sigma_f(z)$ in terms of the axial strain and integrating with respect to distance z . The fibre displacement $u_f(z)$ along the debonded length L , where $0 \leq z \leq L$, is governed by

$$\begin{aligned} E_f u_f(z) &= \sigma(z-L) + \frac{\tau_f(z^2 - L^2)}{a} \\ &+ \frac{2a\tau_d}{\rho^2} + \sigma'_f \left(L - \frac{a}{\rho}\right) \end{aligned} \quad (11)$$

We assume that the residual fibre stress $\sigma'_f < \sigma'_{fc}$ is lower than a critical value that causes spontaneous self-debonding of the composite interface. This critical value σ'_{fc} is given by

$$\sigma'_{fc} = \frac{2\tau_d}{\rho} = \frac{2\tau_f}{\rho} + \frac{4}{\rho} \left(\frac{2G\Gamma_d}{a}\right)^{1/2} \quad (12)$$

The displacement u of the indenter is obtained by evaluating the fibre displacement $u_f(z)$ in Equation 11 at $z = 0$. For this purpose, we express the debond length L in Equation 11 in terms of the applied stress

σ and the shear stress τ_d by using Equation (8). Subsequently expressing σ and τ_d in terms of the applied force P and the interface debond energy Γ_d by using Equations 5 and 9, respectively, we derive the relationship between the force P , the debond energy Γ_d , and the indenter displacement u as

$$\frac{u}{a} = \frac{u_f(0)}{a} = \frac{(P/(\pi a^2) + \sigma'_f)^2}{4\tau_f E_f} - \frac{\sigma'_f}{\rho E_f} - \frac{(8G\Gamma_d/a) - \tau_f^2}{\rho^2 \tau_f E_f} \quad (13a)$$

This relationship is valid only for positive values of the force P after debonding initiates, i.e. $L > 0$. For convenience, we rearrange Equation 13a to express the applied force P in terms of the displacement u as

$$\frac{P}{\pi a^2} = -\sigma'_f + 2\left(\frac{\tau_f E_f u}{a} + \frac{\tau_f \sigma'_f}{\rho} + \frac{(8G\Gamma_d/a) - \tau_f^2}{\rho^2}\right)^{1/2} \quad (13b)$$

Both expressions (Equations 13a and b) are similar to the equivalent relations in Marshall and Oliver [7]. The differences are not substantial, and are because of the fact that we have included the elastic strain energy changes in the bonded region in our analysis in contrast with Marshall and Oliver [7]. The indenter displacement u in Equation 13a is a function of the debond length L . For convenience, we will give its two limiting values u_0 and u_t for two specific debond lengths $L = 0$ and $L = t$, respectively. For this purpose, we evaluate the fibre displacement $u_f(z)$ in Equation 11 at $z = 0$, and express the applied stress σ in terms of the debond length L by using Equation 8. We then set L equal to the specimen thickness t to obtain

$$\frac{E_f u_t}{a} = \tau_f \left(\frac{t}{a}\right)^2 - \frac{\sigma'_f}{\rho} + \frac{2\tau_d}{\rho} \left(\frac{t}{a} + \frac{1}{\rho}\right) \quad (14)$$

and set $L = 0$ to obtain

$$\frac{E_f u_0}{a} = \frac{2\tau_d}{\rho^2} - \frac{\sigma'_f}{\rho} \quad (15)$$

The corresponding force limits P_t and P_0 at $L = t$ and $L = 0$, respectively, are obtained from Equation 11 as

$$\frac{P_0}{\pi a^2} = \frac{\rho E_f u_0}{a} \quad (16)$$

$$\frac{P_t}{\pi a^2} = \frac{P_0}{\pi a^2} + \frac{2\tau_f t}{a}$$

The limiting values (u_0, P_0) and (u_t, P_t) are represented by the points A and B in Fig. 3 where we sketch typical load–displacement curves for the first and the second fibre push. It can be shown that the initial elastic region OA in Fig. 3 is a linear relationship between P and u with a slope $\rho E_f \pi a$, as may be evident from the relationship between P_0 and u_0 in Equation 16. Whether we detect the inflection point A experimentally depends on the observed slope change in the experimental load–displacement curve. The present model predicts a slope change in dP/du , which is a function of the interface bonding Γ_d and can be

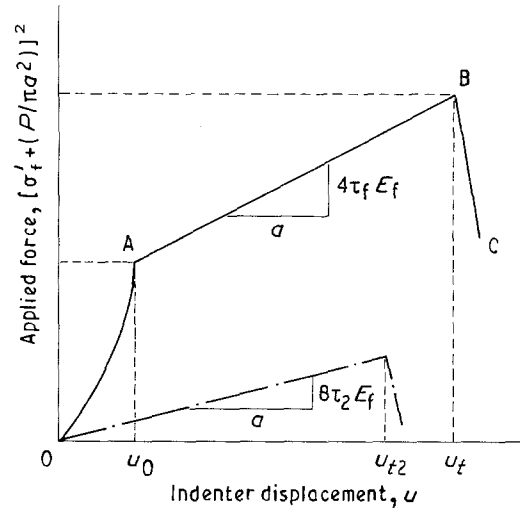


Figure 3 Sketch of the expected load–displacement curves from the model for (—) the first and (---) the second fibre push. The region OA is elastic and debonding is completed at the point B. An initial elastic region exists for the second push also but it is very small ($\sigma'_f = 0$ for the second push).

obtained from Equation 13b as

$$\frac{\text{slope}(-)}{\text{slope}(+)} = \frac{\tau_d}{\tau_f} \quad (17)$$

where $(-)$ and $(+)$ designate the slope to the left and to the right of the point A in Fig. 3. At low values of Γ_d (see Equation 9) the slope change may not be noticeable, depending on the predicted value from Equation 17. If there is an experimentally observed point A during the first fibre push, then the corresponding load or displacement values P_0 or u_0 can be used to calculate the cohesive interface bond energy Γ_d by using Equations 9, 15 and 16.

The frictional stress value τ_f for the first push can be calculated from the slope of the straight portion AB in Fig. 3, using Equation 13a or using the second equation in Equations 16.

3.5. Modelling of the second push

After the first push, the specimen in Fig. 1a is turned over and pushed in the reverse direction. The following differences are noted as compared to the first push case:

1. The interface bonding no longer exists. Therefore, $\Gamma_d = 0$.
2. The frictional characteristics are modified because of the interface damage. The new value of the interface frictional stress, denoted by τ_2 , may differ from the initial frictional shear stress τ_f (see Fig. 3).
3. The original processing-related residual fibre axial stress σ'_f is relieved during the first push. The residual fibre stress for the second push varies linearly with distance z up to a maximum value at the specimen midpoint where $z = t/2$ (see Fig. 4a, following Marshall and Oliver [7]). We assume that the slope of the residual stress profile is governed by the modified frictional stress τ_2 which is assumed to be constant over the entire fibre length.

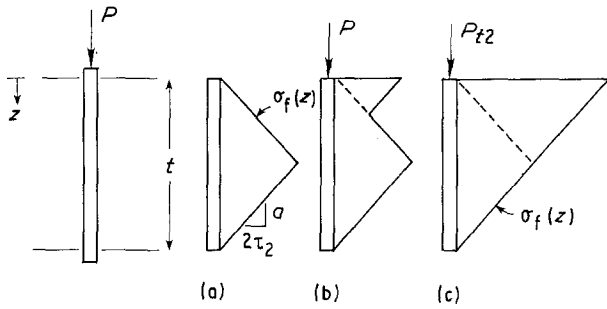


Figure 4 Schematic diagrams showing (a) residual axial stress in the fibre after the first push, (b) variation of the axial stress as the fibre is being pushed a second time, and (c) complete sliding during second push at the maximum load P_{t2} (see Marshall and Oliver [7]).

As a result of these changes, the load–displacement curve for the second push may not exhibit a noticeable initial elastic region (Fig. 3). The indenter displacement that results from reapplying the force P during the second push is denoted by u_2 , and measured with respect to the reference state shown in Fig. 4a. The axial fibre stress profile, as shown in Fig. 4b, has a piecewise constant slope governed by the modified interface shear stress τ_2 . When the applied force P reaches a maximum value P_{t2} , then interface sliding occurs along the entire fibre length as shown in Fig. 4c. The value of P_{t2} is obtained from Equation 8 as

$$\frac{P_{t2}}{\pi a^2} = 2\tau_2 \left(\frac{t}{a} + \frac{1}{\rho} \right) \quad (18)$$

which is the maximum force that can be resisted by the interface frictional stress τ_2 along the fibre length t .

The value of the indenter displacement u_{t2} when the applied force P reaches a maximum is given by

$$\frac{E_f u_{t2}}{a} = \frac{\tau_2}{\rho^2} + \frac{\tau_2}{2} \left(\frac{t}{a} + \frac{1}{\rho} \right)^2 \quad (19)$$

The displacement u_{t2} is the actual indenter displacement as measured from the beginning of the second push. The residual displacement of the fibre that remains after the first push is excluded.

When the force P is less than P_{t2} , the relationship between P and the indenter displacement u_2 is given by

$$\left(\frac{P}{\pi a^2} \right)^2 = 8\tau_2 \left(\frac{E_f u_2}{a} - \frac{\tau_2}{\rho^2} \right) \quad (20)$$

which is sketched linearly in Fig. 3 for $\sigma'_f = 0$.

If the specimen is turned over and the fibre pushed a third time, the frictional interface shear stress assumes a new value τ_3 . Equations 18 to 20 above are unchanged except that τ_2 is replaced by τ_3 . The results given for the second push are close to the corresponding results from Marshall and Oliver [7]. The differences are the $1/\rho$ and τ_2/ρ^2 terms in Equations 18 and 19.

4. Results and discussion

4.1. Fibre push-out tests

Fibre push-out tests were performed on zircon–SiC composites with two types of fibre–matrix interface (A: uncoated fibre and B: BN-coated fibre). Typical load–deflection results for samples containing uncoated Avco SiC filaments are shown in Fig. 5. The data for the first push show a nearly linear portion in which the load increases until the point of filament motion or sliding. Although the peak load is quite reproducible, the experimental slope is not accurate because of the compliance of the testing set-up. This makes it difficult to assess whether there is a slope change during the loading or whether the behaviour is linear or parabolic. A change in the slope, while the load increases, would be a clear evidence of bonding at the interface. Beyond the point of peak load, a sudden drop in load is observed followed by a secondary load increase because of the indenter contacting the matrix material after some fibre sliding has taken place. This composite was then turned over, and the already pushed filaments were pushed for the second time. In this case, again a nearly linear load–deflection relationship is observed, although the slope is somewhat less than in the first push case. The peak load in the

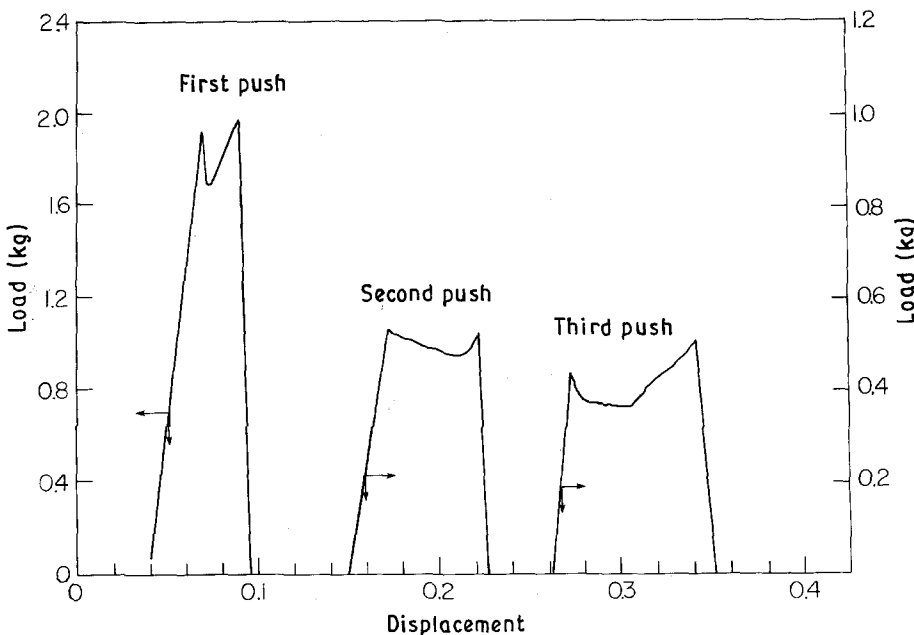


Figure 5 Indenter load–displacement curves for a zircon–SiC composite reinforced with uncoated filaments. The experimental set-up did not produce accurate measurements for the displacements. Displacement rate $0.0508 \text{ mm min}^{-1}$.

second push test is invariably lower than the peak load for the first push. The load drop that occurs after the peak load is more gradual in comparison with the load drop in the first push case. After a significant amount of the filament sliding, the indenter again contacted the matrix phase and led to an increase in load. This sample was then turned over again and pushed for the third time. There is only a small decrease in the peak load when the fibre is pushed for the third time. In all cases, a somewhat higher load was required to initiate filament motion than to sustain it, indicating that the dynamic friction may be lower than the static friction.

Table I gives a summary of sample thickness and an average of maximum force values needed to initiate filament motion in each of the fibre push-out tests. The average force required to initiate filament motion for the first time, in composites reinforced with as-supplied SiC filaments and with $t/a = 14.6$, is 18.23 N, which is much higher than the average value of 7.55 N measured for the second push. There is only a small decrease in force (from 7.55 to 6.96 N) when these filaments were pushed for the third time. This small decrease in interfacial shear stress can be attributed to additional damage at the sliding interfaces resulting from repeated push-out tests.

Zircon composites reinforced with BN-coated SiC filaments (interface B) required lower values of the push-out force to initiate interfacial sliding, as shown

in Fig. 6. However, the nature of the load-deflection data was similar to that observed for composites reinforced with as-supplied SiC filaments. The force required to initiate sliding for the first time (first push) in samples with $t/a = 12.9$ is 7.25 N, which is higher than the force required to initiate sliding for the second (6.08 N), and the third times (6.08 N), as given in Table I. However, in this case the difference in force required to initiate sliding for the first push and the subsequent push is insignificant (compare 7.25 N with 6.08 N). This may be an indication of less damage at this interface than in the uncoated case.

A significantly higher force (18.25 N) for the first push was required to initiate filament sliding in composites reinforced with uncoated SiC filaments in comparison with a force of only 7.25 N that was needed to initiate sliding in composites reinforced with BN-coated SiC filaments. Examination of pushed fibres by an SEM revealed that the interfacial sliding in samples reinforced with uncoated SiC fibres was between the two carbon layers, whereas it was between the BN coating and the zircon matrix in the case of composites containing BN-coated SiC fibres [5]. This explains different values of the force required for interfacial sliding in these two composites.

The influence of the stressing rate on measured values of the interfacial shear stress was studied by pushing on the filament at two different speeds using the indenter and recording the load-deflection data as

TABLE I Summary of experimental results from fibre push-out tests^a

Fibre coating	Sample thickness/ fibre radius t/a	Average push-out load, P_i (N)		
		First push	Second push	Third push
None	14.6	18.23	7.55	6.96
BN	12.9	7.25	6.08	6.08
BN	12.9	—	5.88 ^b	5.88 ^b
None	29.0	35.90	18.40	—
BN	27.9	8.30	7.80	7.60

^a Zircon matrix, SiC fibres. Composite parameters: $V_f = 0.25$, $a = 70 \mu\text{m}$, $E_m = 195 \text{ GPa}$, $E_f = 400 \text{ GPa}$, $G = 78 \text{ GPa}$, $\sigma_f' = 0.0$ (because the fibre and the matrix expansions are both equal to $4.2 \times 10^{-6} (^\circ\text{C})^{-1}$).

^b Tested at a displacement rate of $0.508 \text{ mm min}^{-1}$. Rest of the samples tested at $0.0508 \text{ mm min}^{-1}$.

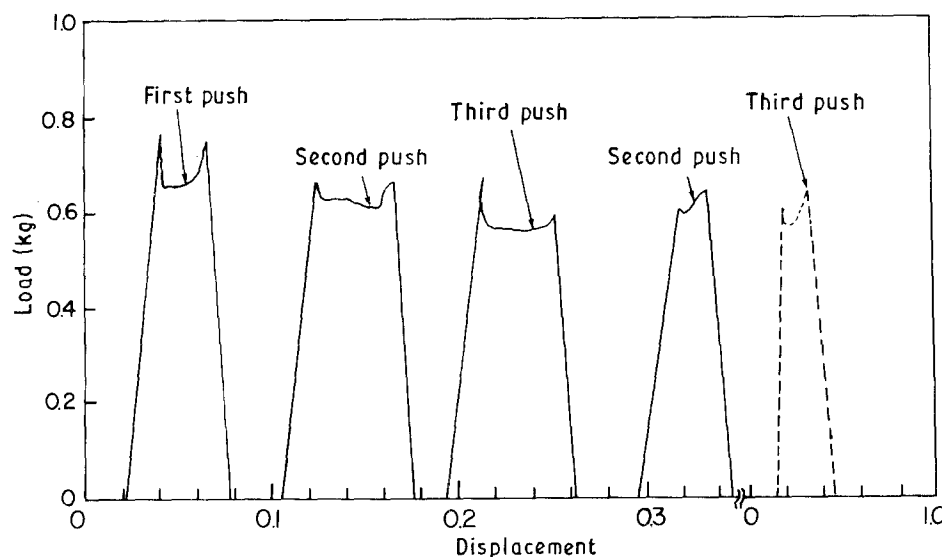


Figure 6 Indenter load-displacement curves for a zircon-SiC composite reinforced with BN-coated filaments. The experimental set-up did not produce accurate measurements for the displacements. Displacement rate (—) $0.0508 \text{ mm min}^{-1}$, (---) $0.508 \text{ mm min}^{-1}$.

given in Fig. 6. A force of 5.88 N was measured when a filament was pushed at a crosshead speed of $0.0508 \text{ mm min}^{-1}$ for the second push, and a force of 5.88 N was also measured on the same filament when it was pushed for the third time at a crosshead speed of $0.508 \text{ mm min}^{-1}$. These results indicate that there is no effect of loading rate on interfacial shear stress values for composite samples reinforced with BN-coated SiC filaments. A similar behaviour was also observed in composites reinforced with as-supplied SiC filaments. These results may suggest an absence of the static fatigue type of crack growth process in this class of composites, but more experiments at very low stressing rate need to be performed to confirm this behaviour.

4.2. Comparison with analytical model

Two types of force–displacement curve are predicted for composite samples depending on the nature of the fibre–matrix interfacial bonding. In a chemically bonded system, a change in slope is predicted (Fig. 3) as the fibres are pushed for the first time in a push-out test in such a way as to initiate debonding as well as frictional sliding. However, once completely debonded these samples should show no change in slope (except for an elastic loading) when pushed for the second time because of the presence of only frictionally coupled fibre–matrix interface. Experimental results from fibre push-out tests on thinner samples ($t/a = 12.9$ to 14.6) show no detectable change in slope while the load increases (Figs 5 and 6). This may be an indication of weakly bonded fibre–matrix interfaces in both composite samples. An analytical estimate of the slope change, for a given interface debond energy Γ_d , can be made from Equation 17 using Equation 9, as given below.

Let us examine two limiting cases of interface bonding and predict the corresponding force values. One limiting case is when the interface debond energy $\Gamma_d = 0$, and the behaviour during the first push is purely frictional. This case predicts an upper bound to the frictional interface shear stress τ_f (from Equation 10), and the results are given in Table II. A shear stress value of 39 MPa for interface A and a value of 17 MPa for interface B are predicted for the first push tests. The corresponding force ratios P_0/P_t , displacement

ratios u_0/u_t , and displacement u_t/a are very small, as shown in Table II, which suggests that it will be difficult to detect a slope change because of the poor accuracy of the test set-up. Similarly, interfacial shear stresses of 16 and 15 MPa are predicted in the second push for interfaces A and B, respectively. Similar values are predicted in the third push tests.

The second limiting case is obtained when the first push frictional stress τ_1 is set equal to the second push frictional stress τ_2 . The calculated interface debond energy Γ_d for the second case will be an upper bound as predicted by Equation 10. The results are summarized in Table III. An interface debond energy of 39 J m^{-2} is predicted for the composite with interface A and a value of 0.35 J m^{-2} is calculated for interface B. The first value of 39 J m^{-2} is unusually large and is close to the matrix fracture energy for crystalline ceramics. Such a large value of Γ_d is expected to produce a slope change by a factor of 37.5 which is not seen experimentally. Similarly, a debond energy of 0.35 J m^{-2} is predicted as an upper bound for interface B, which will lead to a slope change by a factor of 4.7. The actual values of the debond energy in these composites are much smaller than these upper bounds because a slope change was not experimentally observed. These results indicate that the interface bonding in these composites is more likely to be frictional. The higher value of the force needed to initiate sliding at interface A in comparison with that at interface B is because of the interlocking between two carbon layers on Avco SiC fibres as a result of the surface asperities. This type of interlock is broken because of interfacial sliding, which leads to a decrease in contact area and hence a smaller force during subsequent push-out tests. Interface B, between the BN coating and the zircon matrix, is naturally unlocked because of the rough zircon surface that was produced by sintering in contact with the BN coating. This results in lower values of the force in the fibre push-out tests.

Fibre push-out tests were also performed on thicker (2 mm) composite samples in order to increase the accuracy of the push-out force measurements, and to increase the chances of detecting the force P_0 for partial debonding. The nature of the load–deflection curves for composite samples reinforced with uncoated and BN-coated SiC filaments was similar to those shown in Figs 5 and 6, i.e. no evidence of a slope

TABLE II Calculated values of the frictional interfacial shear stress (τ_f), force (P) and displacement (u) as measured from the fibre push-out model assuming unbonded interface ($\Gamma_d = 0$) and using the data in Table I^a

Push-out sequence	Parameter	Uncoated fibres		BN-coated fibres	
		$t/a = 14.6$	$t/a = 29.0$	$t/a = 12.9$	$t/a = 27.9$
First Push	τ_f (MPa)	39	39	17	9.5
	P_0/P_t	0.039	0.020	0.044	0.021
	u_t/a	0.023	0.086	0.008	0.019
	u_0/u_t	0.006	0.0016	0.008	0.0017
Second Push	τ_2 (MPa)	16	20	15	8.9
	u_t/a	0.005	0.022	0.004	0.009
Third push	τ_3 (MPa)	15	–	15	8.6
	u_t/a	0.005	–	0.004	0.008

^a $\rho = 1.7$, displacement rate = $0.0508 \text{ mm min}^{-1}$.

TABLE III Calculated upper bounds for the interface debond energy (Γ_d) assuming the first push frictional stress τ_f equal to the second push value τ_2 , with debond shear stress τ_d and corresponding load and displacement values (material data given in Table I)

Parameter (assumed or calculated)	Uncoated fibres, $t/a = 14.6$	BN-coated fibres, $t/a = 12.9$
$\tau_f = \tau_2$ (MPa)	16	15
P_1 (N)	18.23	7.25
Γ_d (J m ⁻²)	39	0.35
τ_d (MPa)	600	71
P_0/P_1	0.61	0.18
u_f/a	0.036	0.009
u_0/u_f	0.03	0.014

change was found. This is a further indication of purely frictional fibre-matrix interfacial coupling in these composite samples containing uncoated and BN-coated SiC filaments.

A summary of fibre push-out test results for thicker composite samples is also given in Table I. An average force of 59 N for complete sliding was needed for first-push tests in the composite reinforced with uncoated filaments. The second push of these same filaments resulted in a significantly lower force of only 18.4 N for filament sliding. In contrast, a force of only 8.3 N was required to initiate fibre-matrix interfacial sliding in the composite containing BN-coated filaments when pushed for the first time. There was only a small change in the force (from 8.3 to 7.8 to 7.6 N) required for subsequent interfacial sliding of these already-pushed filaments.

The frictional interfacial shear stress τ_f and the force and displacement ratios for the thicker sample are also summarized in Table II. The first-push results give a value of 39 MPa for interfacial shear stress, a value similar to that obtained for the thinner sample. The second and third push-out tests result in a value of 20 MPa for interfacial shear stress in the thicker sample with uncoated filaments. The force and displacement ratios (P_0/P_1 and u_0/u_f) are again very small (Table II) because of the frictionally coupled interface.

An average interfacial shear stress of 9.5 MPa was calculated from the first push force for the BN-coated interface. Similar calculations gave interfacial shear stress values of 8.9 and 8.6 MPa for the second and third push, respectively. The fact that the load drop is insignificant is in agreement with the results from the thinner samples. Commensurate with these results are low values of the force and displacement ratios, as given in Table II.

The experimental anomaly that we are not able to explain at this point is the fact that the load required to push the BN-coated filaments in the thicker samples produced a frictional shear stress $\tau_f = 9.5$ MPa, which is lower than the corresponding value of $\tau_f = 17$ MPa from the thinner samples. We would actually expect the frictional shear stress τ_f to be slightly higher than for the thinner samples because of the Poisson's ratio effects. This experimental anomaly is not observed with the uncoated filaments.

5. Conclusions

A concentric cylinder model was developed for the fibre push-out technique to analyse the experimental observations in fibre push-out tests performed on specimens of zircon-matrix composites uniaxially reinforced with either uncoated or BN-coated SiC filaments. Some of the important conclusions of this study are given below.

1. Modelling of the fibre push-out test resulted in analytical expressions relating the indenter load and displacement. A slope change in the load-displacement data was predicted for composites in which the fibre-matrix interface was initially chemically bonded. In contrast, a very small slope change was predicted for composites in which the fibre-matrix interface was frictionally coupled.

2. The development of an analytical model in concert with experimental determination of the critical loads (P_0 , P_1) and/or the critical displacements (u_0 , u_f) from load-displacement data can be used to calculate the fibre-matrix interfacial debond energy (Γ_d) and the interfacial shear stress (τ_f).

3. The load-deflection curves obtained during push-out tests performed on zircon composites reinforced with uncoated or BN-coated SiC filaments did not display any evidence of the slope change, which suggested that the fibre-matrix interface in these composites was frictionally coupled, i.e. the interface debond energy was very small.

4. Composites reinforced with uncoated SiC filaments produced a much higher interfacial shear stress value of 39 MPa for the first push in comparison with values between 15 and 20 MPa for the subsequent push-out tests. In contrast, composites reinforced with BN-coated filaments produced lower interfacial shear stress values between 15 and 17 MPa for the first, as well as the subsequent push-out tests. These differences were consistent with the different locations of the fibre-matrix interfacial sliding in these composites. Interfacial sliding in composites reinforced with uncoated filaments was between the two carbon coatings, whereas it was between the BN coating and the zircon matrix in composites containing BN-coated filaments.

Acknowledgements

The authors wish to thank W. H. Morrison for his help in sample preparation and P. M. Breslin for preparation of this manuscript. Dr W. B. Hillig read the manuscript and made helpful suggestions.

References

1. B. BUDIANSKY, J. W. HUTCHINSON and A. G. EVANS, *J. Mech. Phys. Solids*, **34** (1986) 167.
2. M. SUTCU, *Acta Metall.* **37** (1989) 651.
3. R. N. SINGH and A. R. GADDIPATI, *J. Amer. Ceram. Soc.* **71** (1989) C100.
4. R. N. SINGH, *Mater. Res. Soc. Symp. Proc.* **5** (1988) 259.
5. *Idem*, *J. Amer. Ceram. Soc.* **72** (1989) 1764.
6. R. N. SINGH and A. R. GADDIPATI, *J. Mater. Sci.* in press.
7. D. B. MARSHALL and W. C. OLIVER, *J. Amer. Ceram. Soc.* **70** (1987) 542.

8. M. K. BRUN and R. N. SINGH, *Adv. Ceram. Mater.* **3** (1988) 506.
9. R. N. SINGH and M. K. BRUN, *ibid.* **3** (1988) 235.
10. J. W. LAUGHNER, N. J. SHAW, R. T. BHATT and J. A. DICARLO, *Ceram. Eng. Sci. Proc.* **7** (1986) 932.
11. C. W. GRIFFIN, D. K. SHETTY, S. Y. LIMAY and D. W. RICHERSON, *ibid.* **9** (1988) 671.
12. U. V. DESHMUKH and T. W. COYLE, *ibid.* **9** (1988) 627.
13. R. N. SINGH, in Proceedings of 10th International Conference on Chemical Vapour Deposition (CVD-X), Honolulu, Hawaii, July 1987, Vol. 87-9, edited by G. W. Cullen (Electrochemical Society, Princeton, N.J., 1987) p. 543.
14. S. P. TIMOSHENKO and J. N. GOODIER, "Theory of Elasticity", 3rd Edn (McGraw-Hill, New York, 1970) pp. 422-425.
15. M. SUTCU and W. B. HILLIG, *Acta Metall. Mater.* **38** (1990) 2653.
16. Z. HASHIN, *ASME J. Appl. Mech.* **46** (1979) 543.

*Received 19 January
and accepted 6 July 1990*